



## OPEN Leveraging cell death patterns to predict metastasis in prostate adenocarcinoma and targeting PTGDS for tumor suppression

Bohong Chen<sup>1,8</sup>, Li Guo<sup>1,8</sup>, Lihui Wang<sup>2,8</sup>, Peiqiang Wu<sup>1,8</sup>, Xinyu Zheng<sup>1</sup>, Congzhu Tan<sup>1</sup>, Na Xie<sup>1</sup>, Xinyue Sun<sup>3</sup>, Mingguo Zhou<sup>1</sup>, Haoxiang Huang<sup>1</sup>, Na Hao<sup>4</sup>, Yangyang Lei<sup>5</sup>, Kun Yan<sup>6</sup>, Dapeng Wu<sup>1,7</sup>✉ & Yuefeng Du<sup>1,7</sup>✉

Metastasis is the major cause of treatment failure in patients with prostate adenocarcinoma (PRAD). Diverse programmed cell death (PCD) patterns play an important role in tumor metastasis and hold promise as predictive indicators for PRAD metastasis. Using the LASSO Cox regression method, we developed PCD score (PCDS) based on differentially expressed genes (DEGs) associated with PCD. Clinical correlation, external validation, functional enrichment analysis, mutation landscape analysis, tumor immune environment analysis, and immunotherapy analysis were conducted. The role of Prostaglandin D2 Synthase (PTGDS) in PRAD was examined through in vitro experiments, single-cell, and Mendelian randomization (MR) analysis. PCDS is elevated in patients with higher Gleason scores, higher T stage, biochemical recurrence (BCR), and higher prostate-specific antigen (PSA) levels. Individuals with higher PCDS are prone to metastasis, metastasis after BCR, BCR, and castration resistance. Moreover, PRAD patients with low PCDS responded positively to immunotherapy. Random forest analysis and Mendelian randomization analysis identified PTGDS as the top gene associated with PRAD metastasis and in vitro experiments revealed that PTGDS was considerably downregulated in PRAD cells against normal prostate cells. Furthermore, the overexpression of PTGDS was found to suppress the migration, invasion, proliferation of DU145 and LNCaP cells. To sum up, PCDS may be a useful biomarker for forecasting the possibility of metastasis, recurrence, castration resistance, and the efficacy of immunotherapy in PRAD patients. Additionally, PTGDS was identified as a viable therapeutic target for the management of PRAD.

**Keywords** Programmed cell death, Prostate adenocarcinoma, Metastasis, PTGDS, Single-cell analysis, Mendelian randomization analysis

Globally, PRAD has consistently remained a prominent research focus in urology, as it exhibits the highest incidence and mortality rates among urothelial malignancies. Worldwide, there are around 375,000 disease-related fatalities and 1.4 million new cases in men each year<sup>1</sup>. PRAD exemplifies indolent tumors, for which active surveillance is often recommended to circumvent adverse outcomes of overtreatment, such as erectile dysfunction and lower urinary tract symptoms<sup>2</sup>. However, radical prostatectomy or radiation therapy, with or without androgen deprivation therapy, is usually necessary for individuals with intermediate or high-risk localized and locally progressed malignancy<sup>3</sup>. Unfortunately, biochemical recurrence occurs in 17–33% of PRAD patients who have radical prostatectomy, and around 30% of individuals acquire metastatic disease<sup>4–9</sup>.

<sup>1</sup>Department of Urology, The First Affiliated Hospital of Xi'an Jiaotong University, Xi'an 710061, Shaanxi, China. <sup>2</sup>Department of Obstetrics and Gynecology, The First Affiliated Hospital of Xi'an Jiaotong University, Xi'an 710061, Shaanxi Province, China. <sup>3</sup>Department of Neurology, The First Affiliated Hospital of Xi'an Jiaotong University, Xi'an 710061, Shaanxi, China. <sup>4</sup>Department of Breast Surgery, The First Affiliated Hospital of Xi'an Jiaotong University, Xi'an 716000, Shaanxi Province, China. <sup>5</sup>Yan'an University, Yan'an 710061, Shaanxi Province, China. <sup>6</sup>Department of Urology, The Second Affiliated Hospital of Xi'an Jiaotong University, Xi'an 710004, China. <sup>7</sup>Department of Urology, First Affiliated Hospital, School of Medicine, Xi'an Jiaotong University, 277 Yanta Western Rd, Xi'an 710061, Shaanxi Province, China. <sup>8</sup>These authors contributed equally: Bohong Chen, Li Guo, Lihui Wang and Peiqiang Wu ✉email: wudapeng1974@163.com; duyuefeng113@163.com

Over 90% of cancer-related fatalities are caused by metastasis, and the majority of individuals with prostate cancer also meet this statistic<sup>10</sup>. The only treatment that can increase survival and quality of life if metastatic prostate cancer is detected is palliative care. Despite several new medications and technologies being developed in recent years, there is still little chance of any kind of cure, particularly for individuals with metastatic castrate-resistant prostate cancer who are in the last stages of the disease<sup>11–13</sup>.

Recently, a growing appreciation for the crucial connection between PRAD and cancer immunotherapy (CIT) has emerged, encompassing checkpoint inhibitors, cytokines, and therapeutic cancer vaccines<sup>14</sup>. For instance, the multicenter immunotherapy for Prostate Adenocarcinoma Treatment (IMPACT) trial evaluated sipuleucel-T, which received Federal Drug Administration approval, in addition to three Phase III clinical trials (NCT00065442, NCT00005947, and NCT01133704). Patients treated with sipuleucel-T exhibited a 3-fold increase in activated T cells within prostatectomy specimens compared to untreated individuals<sup>15</sup>. Moreover, the median survival time for sipuleucel-T recipients was 25.8 months, as opposed to 21.7 months for those administered a placebo. Beer et al. observed a significant difference in progression-free survival (PFS) between ipilimumab and placebo-treated patients, with 5.6 months for the former group and 3.8 months for the latter<sup>16</sup>. Despite the sustained clinical efficacy of CIT, most patients unfortunately do not derive benefit from these approaches<sup>17</sup>. Consequently, identifying a biomarker that accurately predicts metastasis, recurrence, and CIT response for prostate cancer has emerged as a primary objective, which holds significant potential for guiding patient management.

Cell death occurs through two principal mechanisms, contingent on the triggering factors. Programmed cell death (PCD) includes complex regulatory systems and a variety of mechanisms, such as apoptosis, disulfidptosis, necroptosis, ferroptosis, pyroptosis, netotic cell death, entotic cell death, lysosome-dependent cell death, parthanatos, autophagy-dependent cell death, oxeiptosis, and alkaliptosis<sup>18</sup>, whereas accidental cell death (ACD) is an uncontrollable biological event. It has been known for decades that programmed cell death is a crucial factor in the formation and metastasis of malignant tumors. Cancer cells cannot proliferate unless they can overcome several types of cell death<sup>19,20</sup>. However, a comprehensive understanding of the relationship between PCD and PRAD remains elusive, with relatively little investigation of the specific roles played by PCD in PRAD. Consequently, this study aimed to establish a novel indicator, the PCD score (PCDS), to simultaneously predict metastasis, recurrence, and immunotherapeutic efficacy of PRAD. Additionally, we examined the role of PTGDS in the progression of prostate cancer and assessed its therapeutic target potential.

## Materials and methods

### Data sources and model development

The workflow of this study is illustrated in Fig. S1. The present study analyzed a comprehensive set of 1267 genes associated with PCD (Supplementary Table 1), which were sourced from diverse resources such as GSEA gene sets, KEGG, review articles and manual curation. Among them, 580 genes were related to apoptosis, 15 to disulfidptosis, 52 to pyroptosis, 88 to ferroptosis, 367 to autophagy, 15 to entotic cell death, 101 to necroptosis, 14 to cuproptosis, 9 to parthanatos, 8 to netotic cell death, 7 to alkaliptosis, 220 to lysosome-dependent cell death, and 5 to oxeiptosis<sup>18</sup>.

In the TCGA-PRAD cohort, raw transcriptome counts of 499 PRAD patients and 52 matched normal tissues were generated. Then, using the criteria  $P < 0.05$  and  $|\log_2FC| > 1$ , the “DESeq2” package was utilized to filter out DEGs. The resulting differentially expressed genes intersected with 1156 genes from 13 cell death modes, resulting in 98 candidate genes (Supplementary Table 2). Using Lasso and Cox regression analysis, 248 samples with full clinical data in GSE116918 were utilized to identify the final genes<sup>21</sup>. To determine if these genes affected the metastatic status of PRAD, univariate Cox regression was used. We modified the cut-off P-value at 0.1 to prevent omissions (Supplementary Table 3). To create the best possible signature, the choices were further reduced using the LASSO Cox regression approach, and the “lambda. min” value was chosen (“glmnet” R package). In the end, each patient’s PCDS was exported by the model using the following formula:

$$PCDS = \sum_{i=1}^n \beta_i * E_i.$$

The risk coefficient is represented by  $\beta_i$ , while each gene’s expression is shown by  $E_i$ . Based on the median PCDS, we classified the patients into high- and low-PCDS groups.

GSE21034<sup>22</sup> and GSE134051<sup>23</sup> were used to validate the diagnostic and prognostic values of PCDS based on definitive genes. Moreover, we assessed the recurrence using the GSE116918 and TCGA-PRAD cohorts and tested the ability of the PCDS to predict CTRP using the GSE35988<sup>24</sup> and GSE28680<sup>25</sup> cohorts.

Datasets from public repositories might be used without the need for informed permission or approval from an ethical review committee. In compliance with the exclusion criteria, individuals lacking prognostic data or expression profiles, as well as those who passed away within 30 days, were not included in this study.

### Functional enrichment analysis

Differential analysis was conducted using the limma package, leveraging the GSE116918 dataset. To investigate the potential biological functions and signaling pathways of these DEGs, we performed GO, Kyoto Encyclopedia of Genes and Genome (KEGG)<sup>26–28</sup>, and gene set enrichment analysis (GSEA) using the R package “clusterProfiler”<sup>29</sup>. We also performed a similar analysis on the PTGDS gene.

### TME and mutation analysis

From a study by Jia et al.<sup>30</sup>, which 28 human immune cell types were preserved, including natural killer T cells, activated CD4 T cells, activated dendritic cells, regulatory T cells, effector memory CD4 T cells, effector memory

CD8 T cells, gamma delta T cells, immature B cells, activated CD8 T cells, central memory CD4 T cells, central memory CD8 T cells, etc. (Supplementary Table 4), we were able to get a gene set designating each TME-infiltrating immune cell type. The relative abundance of each TME-infiltrating cell in each sample was represented by the enrichment fraction determined by ssGSEA analysis. Furthermore, prevalent immune checkpoint markers were included in the current work. Next, we estimated the probability of the immunotherapeutic response using the TIDE method (<http://tide.dfci.harvard.edu>) and the submap algorithm (<https://cloud.genepattern.org/gp>)<sup>29</sup>.

We compared mutational patterns among subgroups by analyzing and visualizing somatic data using the R package Maftools<sup>31</sup>. Furthermore, we utilized the transformation analysis function module to examine the variations in drug-gene interactions and carcinogenic signaling pathways across various subgroups.

### Single-cell sequencing analysis

The GSE141445 provided the single-cell sequencing data for 33,441 cells from 13 human PCa samples. The R package “Seurat” was utilized for the single-cell sequencing samples’ data processing. Following principle component analysis (PCA) with the “RunPCA” function, a K-nearest neighbor was built using the “FindNeighbors” function. The “FindClusters” function was used to integrate cells with the highest gene alteration. Subsequently, cell annotation was carried out using the “SingleR” package.

Downscaling was used to graphically display complex expression profiles, with the “RunTSNE” function making this possible. The substantially differentially expressed genes (DEGs) between the identified microenvironment cells were eliminated by the “FindMarkers” algorithm. Then we conducted pseudotime analysis using the “monocle” R package. Analysis of cell-to-cell interactions was conducted with the “CellChat” R package. An analysis and visualization were conducted on the different interactions between malignant cells expressing high or low levels of PTGDS and other recognized cell types in various receptor-ligand signaling pathways<sup>32</sup>.

### Cell culture and transfection

Human prostate cancer cells DU145 and LNCaP, along with the human benign prostatic hyperplasia cell line BPH-1, were purchased from the American Type Culture Collection (ATCC, Rockville, MD, USA). 0.10% FBS was added to RPMI medium to boost BPH-1, DU145 and LNCaP cultures. By transfecting the PTGDS plasmid (WZ Biosciences Inc., China) with the aid of Lipofectamine 3000 Transfection Reagent (Thermo, USA) by the suggested procedures, the PTGDS was overexpressed in the PRAD cells.

### Cell counting kit-8 assay

The 96-well plates were seeded with 3000 cells per well, and the cells were cultured for 24, 48, 72, or 96 h at 37 °C in 5% CO<sub>2</sub>. After adding 10 µl of CCK8 solution (GlpBio, USA) to each well at the specified time, the OD value was measured at 450 nm using a multi-scan spectrophotometer after two hours.

### Migration and invasion assays

To test PRAD cells’ ability to invade or migrate, a transparent PTFE membrane (Millipore, 8 µm pore size) with or without Matrigel was utilized. In summary, 200 µl of FBS-deficient media was placed in the upper chamber and 2–4 × 10<sup>4</sup> cells were added. Concurrently, a 600 µl media containing 20% FBS was introduced into the lower chamber. The chambers were incubated at 37 °C for 24, 48, or 96 h. Afterward, they were cleaned with PBS and preserved for about 30 min using 4% paraformaldehyde. Following a half-hour staining period at room temperature with crystal violet, the cells on the upper side of the membrane were scraped off. After three PBS washes, the membranes were allowed to dry at room temperature before being photographed.

### Wound healing assay

A 6-well plate was seeded with 1.2 × 10<sup>6</sup> cells per well. After cultivation for 24 h, the cell layer was scraped off using a sterile plastic suction pipette, and the cells were then cultivated in a medium lacking in fetal bovine serum. The photos were taken at 0, 24, or 48 h, respectively. Using ImageJ, the retained area was computed. The change in the wounded area’s size was indicative of the cells’ ability to migrate.

### Total RNA isolation and quantitative RT-PCR

The total RNA extracted from the cells was done so using the TRIZOL reagent (Fastagen, China). Reverse transcription kits (Yeasen, China) were used to generate cDNA utilizing quantified RNA as a substrate by the manufacturer’s instructions. RT-qPCR, or real-time quantitative PCR, was carried out using a Bio-Rad CFX 96 touch (Bio-Rad, Hercules, CA, USA). The formula 2-ΔΔCt technique was utilized to compute the fold changes. β-actin forward, 5'-CCTCGCTCTCCACACCA; β-actin reverse, 5'-GCCAGTCCCATCCACAGT; PTGDS forward, 5'-CCCAGGGCTGAGTTAAAG; PTGDS reverse, 5'-GAGTCCTATTGTCCGTCAT were the PCR primer sequences used for qRT-PCR.

### Western blot

Cells were lysed in RIPA lysis buffer (Beyotime Biotechnology, China) containing protease inhibitor cocktail. BCA protein quantification kit (Solarbio, China) was used to detect the protein concentration. 30 µg protein were separated by SDS-PAGE and then transferred to NC membrane. After blocking with 5% nonfat milk, the membranes were incubated overnight at 4 °C with the indicated primary antibodies, followed by incubation with HRP-labeled secondary antibody for 1 h at room temperature. Primary antibodies used in this study were purchased from ABclonal (E-Cadherine, 1:1000; N-Cadherine, 1:1000; β-Actin, 1:20,000), Zenbio (Slug, 1:1000; PTGDS, 1:1000; Vimentin, 1:1000; β-Catenin, 1:1000; Snail, 1:1000).

## Mendelian randomization analysis

### *eQTLGen consortium*

Genome-wide significant cis-eQTLs (false discovery rate < 0.05) within  $\pm 1$  Mb of probe locations were identified. The dataset utilized for this analysis, eQTLGen, encompasses 16,987 genes and was derived from the analysis of 31,684 blood samples, primarily collected from individuals of European ancestry and characterized by their overall good health. Emphasizing the relevance of eQTLs in drug development studies due to their proximity to the target genes and direct impact on gene expression, we narrowed down our selection to SNPs situated within 100 kb upstream of transcription start sites or 100 kb downstream of transcription end sites of druggable genes. Finally, we conducted an intersection of genes between the eQTLGen Consortium and the PCDS model, resulting in the identification of four genes: ALOX15, CD38, CD68, and PTGDS.

### *GWAS of prostate cancer*

The GWAS data for prostate cancer were sourced from FinnGen Release 10 (<https://www.finnngen.fi/en>)<sup>33</sup>, which was published in December 2023. Prostate cancer in FinnGen was defined based on the International Classification of Disease (ICD), encompassing 15,199 cases, and 131,266 controls.

### *Mendelian randomization analysis*

The TwoSampleMR R package (version 0.5.7, <https://mrcieu.github.io/TwoSampleMR/>) was employed to execute two-sample MR analysis<sup>34</sup>. Stringent quality control of the SNP instruments was implemented before MR testing. First, variants with weak instrument strength ( $F$ -statistic < 10, where  $F = (\text{beta}/\text{se})^2$ ) were excluded. Conditionally independent variants in low linkage disequilibrium (LD  $r^2 < 0.1$  per 1000 Genomes European panel) were then selected. Finally, Steiger filtering removed genes wherein SNPs explained greater outcome than exposure variance.

For proposed instruments that encompassed more than one SNP, a comprehensive approach was adopted. This included the use of the inverse variance weighted (IVW) method, MR-Egger, and weighted median MR. To account for multiple testing in the sensitivity analyses, Bonferroni corrections were implemented to establish adjusted significance thresholds. In the eQTLGen cohort,  $p$ -values below 0.0125 (calculated as  $p = 0.05/4$ ) were deemed significant. Following this, quality control procedures were applied to genes identified as significant, ensuring consistency in the direction of estimated effects across the three methods and confirming the absence of horizontal pleiotropy via the MR-Egger test. Furthermore, a Steiger filtering procedure was executed to confirm the directionality of the association between expression quantitative trait loci (eQTL) and prostate cancer<sup>35</sup>. Statistical significance was established at a threshold of  $P < 0.05$ , providing a rigorous criterion for the validity and reliability of the observed associations.

### *Colocalisation analysis*

For genes with significant Mendelian randomization associations in eQTLGen and cohort, colocalization analysis was performed using the coloc R package with default priors<sup>36</sup>. This Bayesian approach tested whether the gene expression-prostate cancer links were driven by shared causal variants at a given locus rather than linkage disequilibrium. Specifically, five mutually exclusive hypotheses were assessed: (H0) no association with either trait; (H1) association with expression only; (H2) association with disease only; (H3) association with both traits, but independent causal variants; (H4) association with both traits driven by a shared causal variant<sup>37</sup>. Posterior probabilities were furnished for each hypothesis. Prior probabilities were set at  $1E-4$  for trait 1 only ( $p_1$ ) and trait 2 only ( $p_2$ ), and  $1E-5$  for both traits ( $p_{12}$ ).

### *Phenome-wide association analysis*

Utilizing the AstraZeneca PheWAS Portal (<https://azphewas.com/>), a Phenome-Wide Association Study (PheWAS) was carried out to thoroughly evaluate the horizontal pleiotropy of possible therapeutic targets and probable adverse effects<sup>38</sup>. To mitigate the risk of false positives, we implemented multiple corrections and established a significance threshold of  $2E-9$ , as per the default setting in the AstraZeneca PheWAS Portal.

## Statistical analysis

All statistical analyses were conducted via R software (v.4.2.1). Student's  $t$ -test or Wilcoxon test was used to analyze differences between the two groups. Survival curves were described by Kaplan-Meier plots and compared with the log-rank test. Spearman's correlation analysis was used to measure the degree of correlation between certain variables. All statistical tests were two-sided, with  $P < 0.05$  as statistically significant ( $*P < 0.05$ ,  $**P < 0.01$ ,  $***P < 0.001$ ).

## Results

### Construction of a prognostic gene signature for PRAD patients

In the TCGA-PRAD cohort, we identified 2,044 DEGs with  $P$ -values < 0.05 and absolute  $\log_2$  fold change > 1 compared to normal samples. Of these DEGs, 800 were upregulated and 1,244 were downregulated in PRAD, as depicted in Fig. 1A. Furthermore, we have identified 98 tumor-related cell death-related genes by intersecting the differential genes with programmed cell death-related genes, as depicted in Fig. 1B. In order to establish an 8-gene signature, which we refer to as the PCD Score (PCDS), we utilized univariate Cox regression analysis and LASSO Cox regression analysis, drawing upon the GSE116918 cohort as a basis. Of the 8 genes in the signature, BIK, CCK, and CD38 were derived from apoptosis, CD68 and PTGDS were derived from lysosome-dependent cell death, EEF1A2 was derived from autophagy, CDKN2A was derived from cuprotoxicity, and ALOX15 was derived from ferroptosis, as illustrated in Fig. 1C–E. Significant correlations were detected between PCDS and multiple adverse clinical features, including metastasis (Fig. 1F), Gleason score (Fig. 1G), T stage (Fig. 1H),

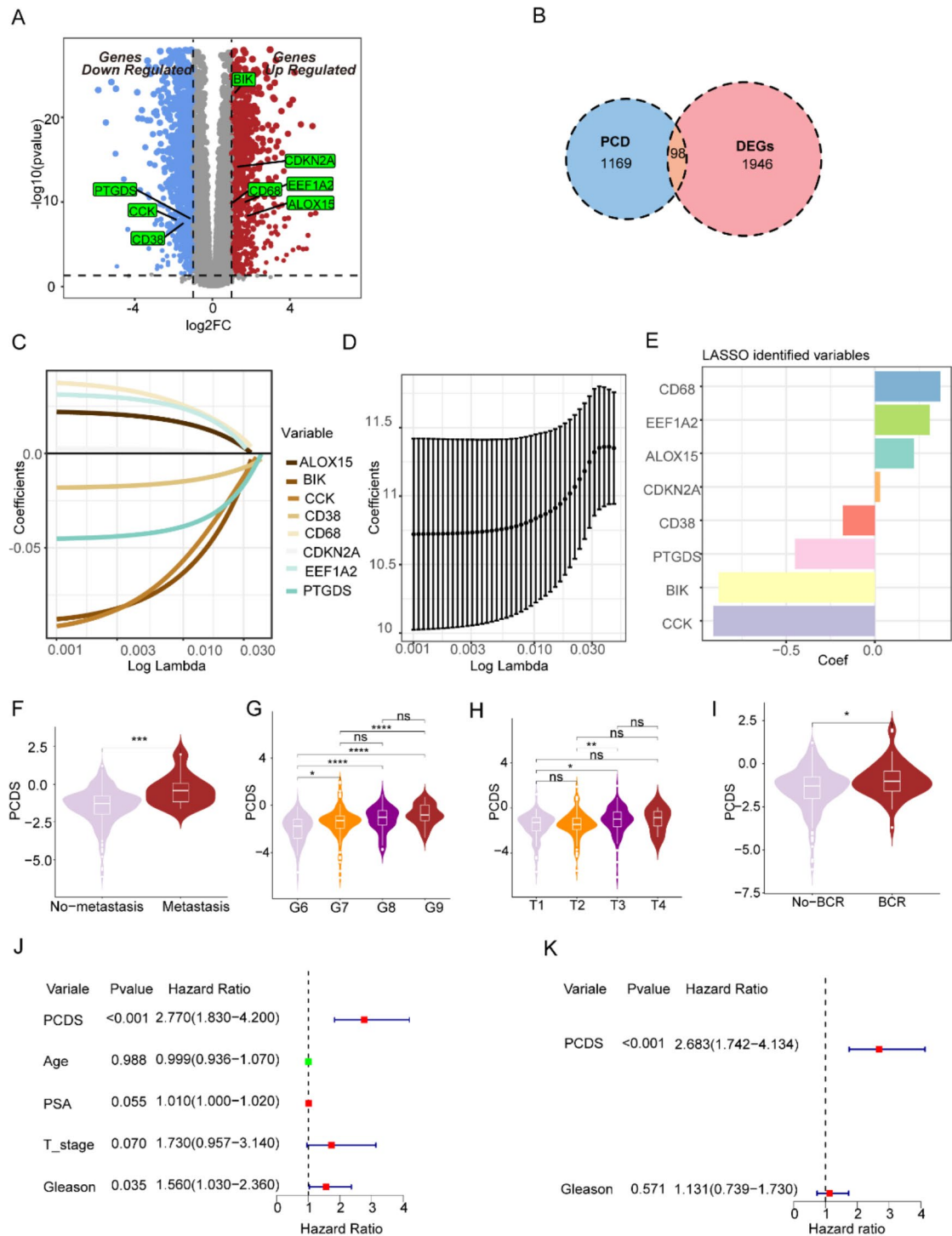


**Fig. 1.** Construction and validation of the PCD-related prognostic model and its association with clinical characteristics. (A) Volcano plot; (B) Venn diagram; (C) Selection of the 8 model genes by Lasso regression method; (D) Cross-validation of the constructed signature; (E) Coefficients for 8 modeled genes; Comparative analysis between the PCDS and metastasis status (F), Gleason score (G), T stage (H), and biochemical recurrence (I); (J,K) Univariate and multivariate Cox analysis of PCDS and clinical parameters for metastasis-free survival. \*\*\*\* $P < 0.0001$ , \*\*\* $P < 0.001$ , \*\* $P < 0.01$ , \* $P < 0.05$ , ns non-significant.

and biochemical recurrence (BCR) presence (Fig. 1I). This trend was further confirmed in our analysis using the two external validation cohorts (Fig. S2). Remarkably, PCDS exhibited independent predictive capacity for metastasis in both univariate and multivariate Cox regression analyses, while accounting for other significant clinical variables (Fig. 1J,K).

### Prediction of MFS and MFS after BCR using PCDS

Our analysis demonstrated that high-PCDS patients faced a greater risk of metastasis compared to low-PCDS patients (Fig. 2A), as well as an increased risk of MFS following BCR (Fig. 2B). The PCDS exhibited exceptional diagnostic accuracy in predicting MFS (Fig. 2C,D) and MFS after-BCR (Fig. 2E,F). Moreover, our findings indicated that PCDS outperformed other clinical variables in metastasis diagnostic accuracy, particularly age and PSA levels ( $p < 0.05$ , Fig. 2G,H). In both the GSE21034 and GSE134051 validation cohorts, PCDS displayed remarkable metastasis diagnostic precision (Fig. 2I,J).

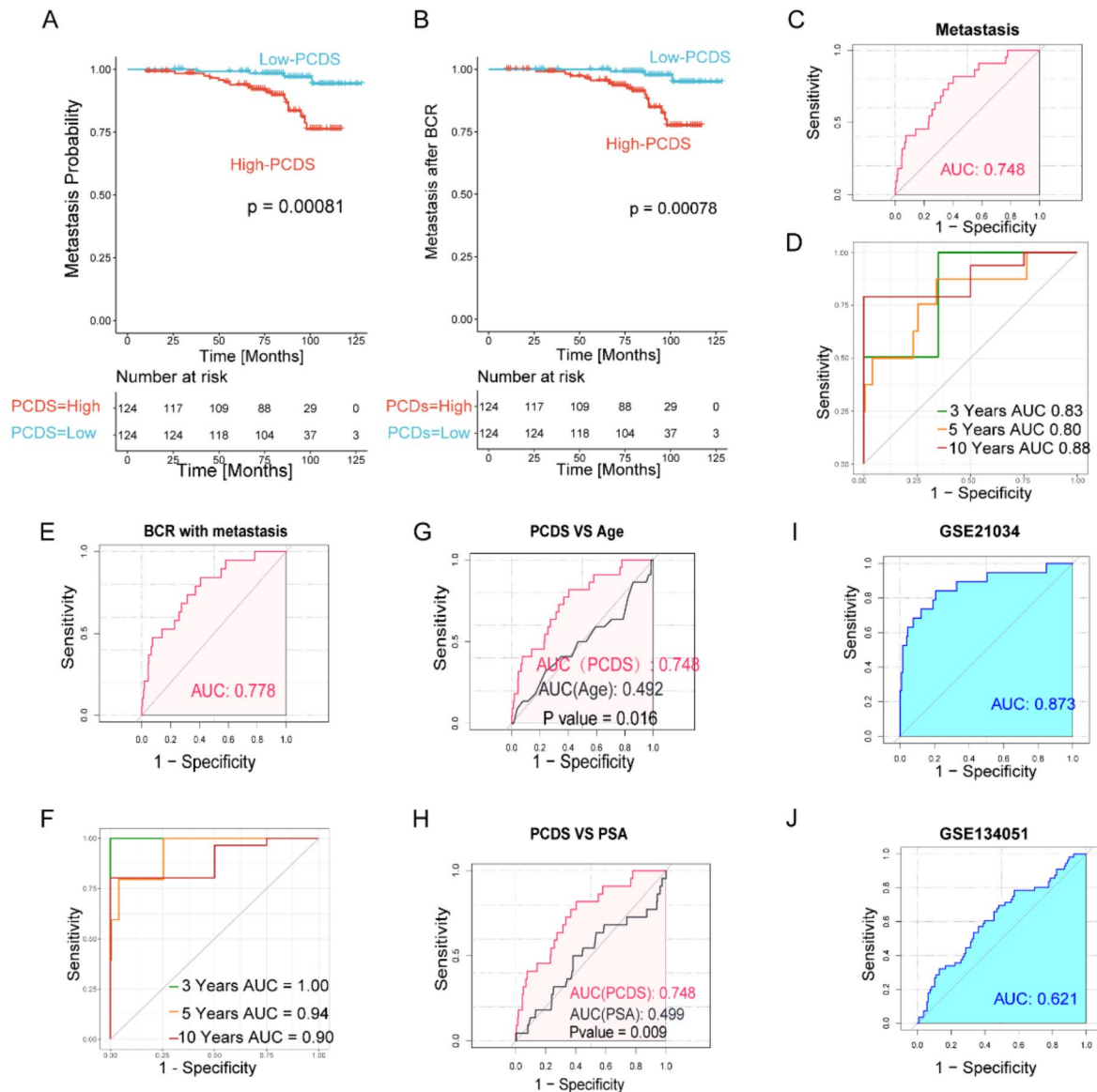


**Fig. 2.** Clinical Relevance of PCDS in Predicting Metastasis. Kaplan–Meier curves illustrating metastasis-free survival (A) and metastasis-free survival after biochemical recurrence (B). ROC curve of PCDS for metastasis (C) and its time-dependent ROC curve (D). ROC curve of PCDS for metastasis after biochemical recurrence (E) and its time-dependent ROC curve (F). Comparison of ROC curves between age and PCDS (G), and between PSA and PCDS (H). ROC curve of PCDS for metastasis using GSE21034 (I) and GSE134051 (J).

### Predicting BCR and CTRP using PCDS

Strikingly, our results suggest that PCDS not only holds the potential to predict prostate cancer metastasis but also demonstrates outstanding performance in predicting and diagnosing recurrence within the GSE116918 cohort (Fig. 3A,B). To further substantiate these findings, we employed the TCGA-PRAD dataset for validation and observed analogous outcomes (Fig. 3C,D). Additionally, PCDS was shown to accurately discern castration-resistant prostate cancer among prostate cancer patients (Fig. 3E,F).

### Function analysis

GSEA analysis demonstrated a positive association between high PCDS and immune-related pathways, including cytokine–cytokine receptor interaction, antigen processing and presentation, natural killer cell-mediated cytotoxicity, and primary immunodeficiency (Fig. 4A). Furthermore, pathways related to tumors, such as those associated with cell cycle, apoptosis, and bladder cancer, were also identified (Fig. 4B). KEGG analysis revealed the involvement of candidate genes in various pathways, including PI3K–Akt signaling pathway, focal adhesion, complement, and coagulation cascades, ECM–receptor interaction, cell adhesion molecules, cell cycle, leukocyte transendothelial migration, platinum drug resistance, p53 signaling pathway, and intestinal immune network for IgA production (Fig. 4C). Additionally, GO analysis indicated the candidate genes' involvement in positive regulation of cell adhesion, wound healing, negative regulation of immune system process, and other biological processes (Fig. 4D).

### Dissection of tumor microenvironment based on PCDS group

Moreover, we conducted an analysis to discern disparities in tumor-infiltrating immune cell populations between the high and low PCDS groups. Utilizing the ssGSEA algorithm, we observed that patients in the high PCDS group exhibited significantly elevated scores for activated dendritic cells, eosinophils, gamma delta T cells, immature dendritic cells, MDSCs, and regulatory T cells compared to their low PCDS counterparts (Fig. 5A). A strong positive connection between PCDS and these immune cells was found using Spearman analysis (Fig. 5B). In accordance with prior research, the prognostically relevant immune cells among these populations included MDSCs and regulatory T cells, both of which have been associated with unfavorable outcomes<sup>39</sup>. This finding may provide an explanation for the worse prognoses of patients in the high-PCDS group compared to those in the low-PCDS group. Remarkably, compared to individuals without metastases, MDSC levels were likewise much higher in patients who had metastases (Fig. 5C). In light of these observations, we hypothesized that MDSCs may play a critical role in prostate cancer metastasis. Patients in the MDSCs-high group exhibited a greater propensity for metastasis compared to the MDSCs-low group (Fig. 5D), and MDSCs demonstrated an accurate predictive capacity for metastasis in prostate cancer patients (Fig. 5E).

### Mutation spectrum characteristics between PCDS group

Apart from the tumor microenvironment, genomic mutations are recognized as critical drivers of metastatic progression<sup>40</sup>. Differential distribution analysis of tumor somatic mutations between the two subtypes was conducted to discern potential distinctions. The PCDS-high subtype exhibited a higher frequency of gene mutations compared to the PCDS-low subtype (Fig. 6A). The top 20 mutated genes are depicted in the figure, with TP53, TTN, and SPOP being the most frequently mutated genes in both subtypes. The PCDS-high subtype displayed a higher mutation frequency for several genes, including TP53 (23.2% vs. 11.3%), TTN (17.5% vs. 16.9%), MUC16 (9.6% vs. 7.3%), LRP1B (8.5% vs. 4.8%), KMT2C (7.3% vs. 5.6%), ATM (6.2% vs. 5.6%), and CACNA1E (5.1% vs. 4.8%). The forest analysis further substantiated these findings (Figure S3A). The fraction of affected pathways and affected samples in the high-PCDS group was more frequent than in the low-PCDS group (Fig. 6B). For example, the high-PCDS subtype exhibited a higher frequency than the low-PCDS subtype for the fraction of affected pathways in RTK-RAS (60/85 vs. 22/85), WNT (42/68 vs. 18/68), NOTCH (31/71 vs. 17/71), and Hippo (24/38 vs. 9/38). The PCDS-high subtype also demonstrated a higher frequency for the fraction of affected samples in RTK-RAS (48/243 vs. 27/241), WNT (41/243 vs. 20/241), NOTCH (35/243 vs. 21/241), and Hippo (43/243 vs. 19/241). To investigate possible therapeutic targets of altered genes, the DGIdb database was utilized. The potential therapeutic targets for the PCDS-low subtype included ATM, BRAF, FOXA1, GRIN2A, and KDM6A, while the PCDS-high targets primarily consisted of ATM, CACNA1E, CNTNAP5, MUC16, and MUC17 (Figure S3B). The somatic interactions analysis, presented in Figure S4, suggests that these co-occurrence and mutually exclusive characteristics could potentially be harnessed for the development of treatments tailored to specific subtypes.

### The PCDS has predictive potential as an indicator of response to CIT

The implementation of immune checkpoint inhibitors targeting PD-L1 and PD-1 has revolutionized cancer treatment, establishing itself as a pivotal advancement in immunotherapy. Our investigation reveals that patients classified in the PCDS-low group exhibit low levels of immunosuppressive molecule LAIR1 (Fig. 7A), as well as lower TIDE and exclusion scores (Fig. 7B), all of which are associated with enhanced responsiveness to immunotherapy. In contrast, the submap algorithm's outcomes imply that the PCDS-high group may exhibit reduced immunotherapy sensitivity (Fig. 7C). These findings substantiate the marked therapeutic superiority and clinical response of patients with low PCDS to anti-PD-1 immunotherapy compared to their high PCDS counterparts.

### PTGDS as a core gene and its role in the PRAD

Among the eight modeling genes, only six demonstrated statistically significant associations with metastasis, as determined by Kaplan–Meier survival analysis: PTGDS, CD68, ALOX15, CD38, BIK, and EEF1A2 (Fig. S5). In order to ascertain the gene with the greatest influence on PRAD metastasis, a random forest analysis was

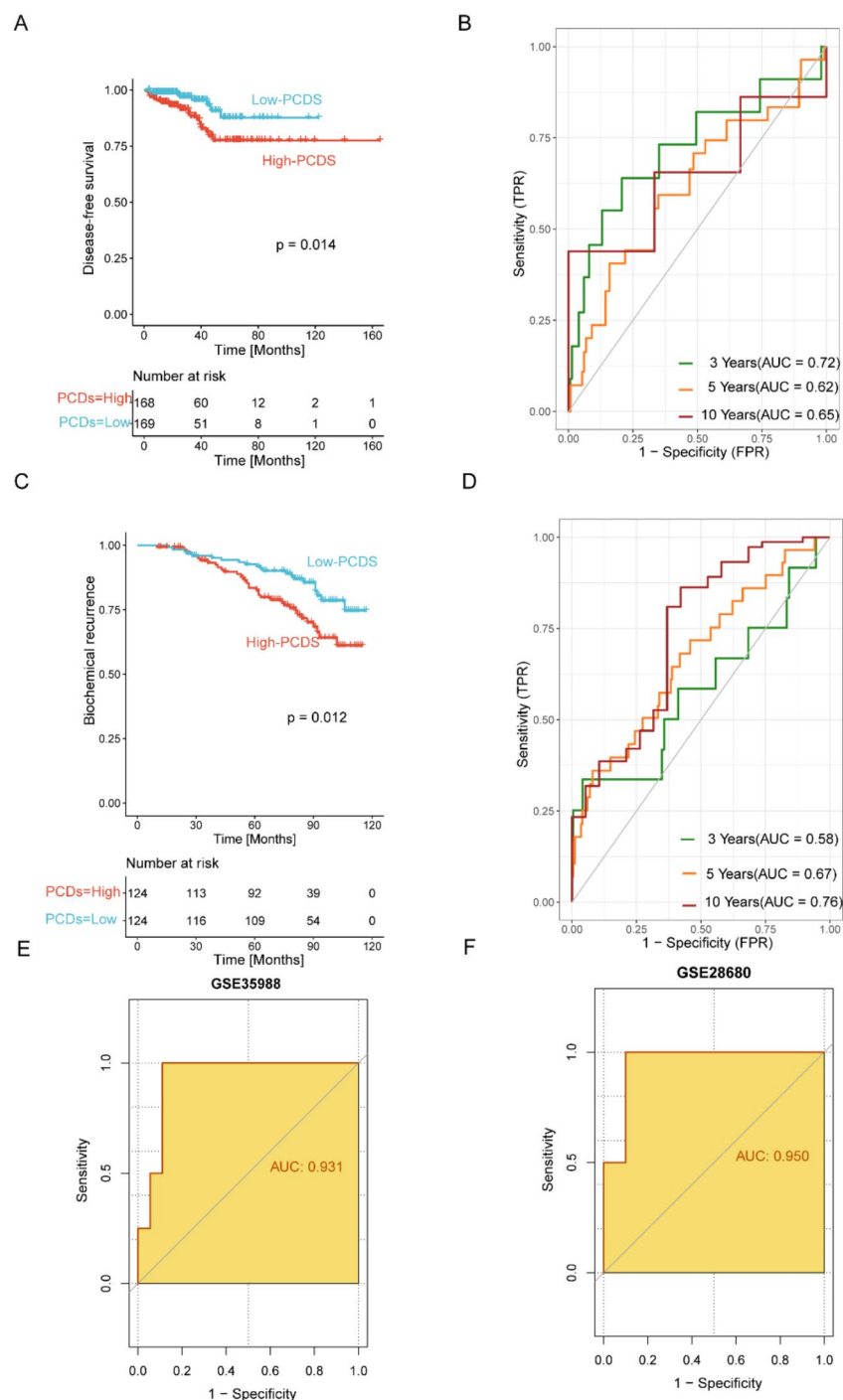


**Fig. 3.** Clinical Relevance of PCDS in Biochemical Recurrence and Castration Resistance. Kaplan–Meier curves depicting biochemical recurrence using GSE116918 cohort (A) and TCGA-PRAD cohort (C). Time-dependent ROC curve of PCDS for biochemical recurrence using GSE116918 cohort (B) and TCGA-PRAD cohort (D). ROC curves of PCDS for castration resistance generated using data from the GSE35988 (E) and GSE28680 cohorts (F).



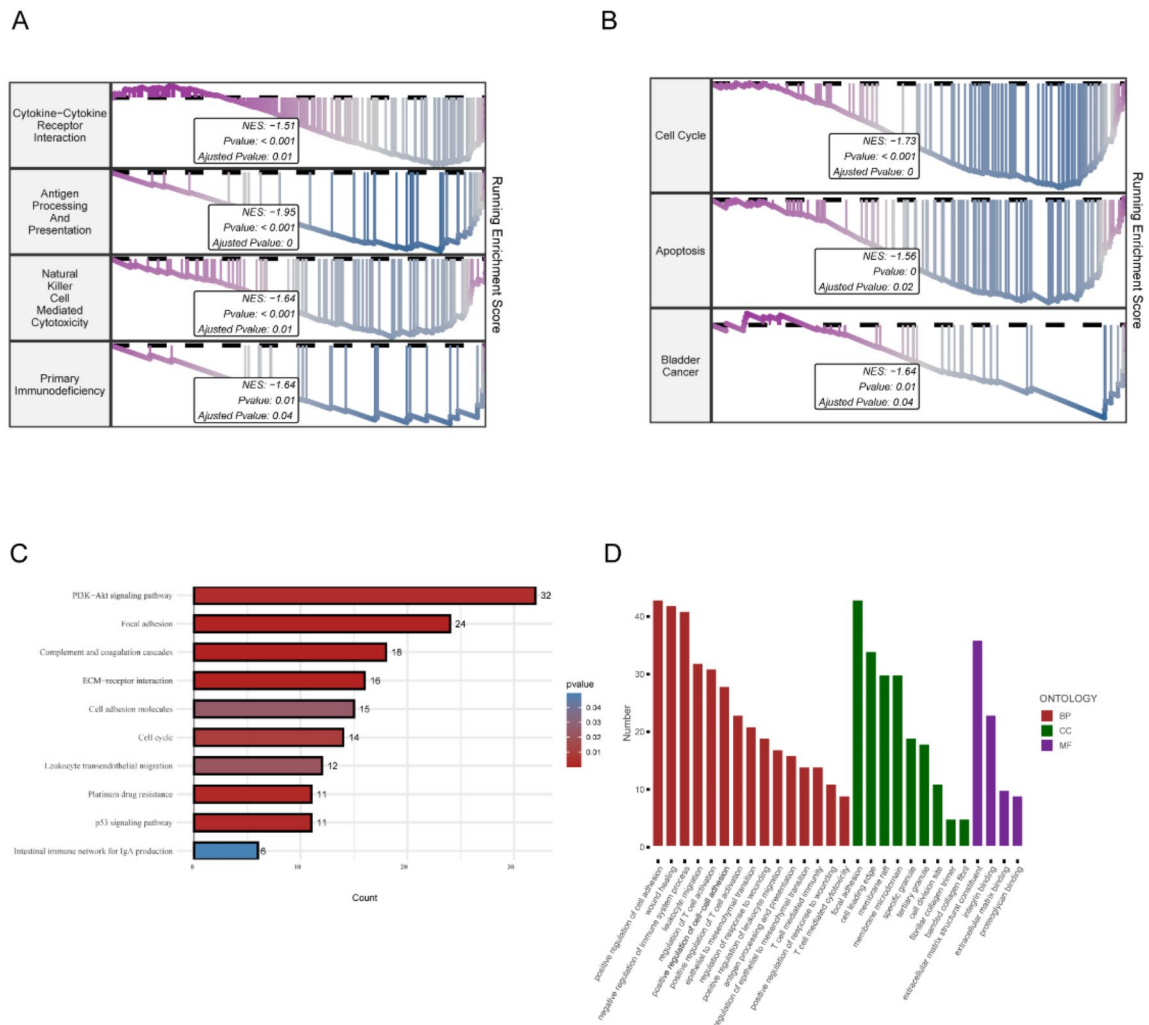


**Fig. 4.** Functional enrichment analysis. (A,B) GSEA; (C) KEGG<sup>26–28</sup>; (D) GO.

conducted, identifying PTGDS as potentially playing a central role (Fig. 8A). Moreover, the area under the receiver operating characteristic (ROC) curves substantiated the high sensitivity and specificity of PTGDS in predicting PRAD metastasis in both the training and validation cohorts (Fig. 8B,C). In both discovery and validation cohorts, PTGDS expression was significantly lower in metastatic versus non-metastatic prostate cancer (Fig. 8D,E). Furthermore, inverse correlations emerged between PTGDS levels and increasing Gleason score, T stage, biochemical recurrence incidence, and PSA levels (Fig. 8F and I), aligning with more advanced disease. PTGDS mRNA expression was examined by qRT-PCR in benign prostatic hyperplasia BPH-1 cells versus prostate cancer DU145 and LNCaP lines. PTGDS levels were significantly reduced in the malignant cells compared to BPH-1 controls (Fig. 8J). The Human Protein Atlas (HPA) database further confirmed substantial downregulation of PTGDS protein in prostate cancer tissues relative to adjacent normal tissue (Fig. 8K). All these results collectively indicate that low PTGDS expression serves as a promising biomarker for predicting aggressive PRAD.

### Unveiling PTGDS as a prospective biomarker using mendelian randomization and colocalization study

The intersection of model genes and drug-related genes resulted in four genes: ALOX15, CD38, CD68, and PTGDS. At Bonferroni significance ( $P < 0.0125$ ), the Mendelian randomization (MR) analysis revealed that only PTGDS is causally related to the risk of PRAD, as illustrated in Fig. 9. PTGDS showed a consistent direction of effect across the three methods and no heterogeneity ( $P > 0.05$ , Table S6) and horizontal pleiotropy ( $P > 0.05$ , Table S6) was detected in the primary analysis. Finally, steiger filtering further ensured directionality ( $P < 0.05$ , Table S7). To study the potential side effects of PTGDS, we used gene expression as exposure and summary statistics of diseases in the UK Biobank cohort ( $n \leq 408,961$ ) as outcomes to perform phenome-wide MR based on AstraZeneca PheWAS Portal database. As illustrated in Fig. S7, PTGDS not show significant associations with other traits at the gene level ( $P < 5E - 8$  for genomic association). This further supports the validity of the study

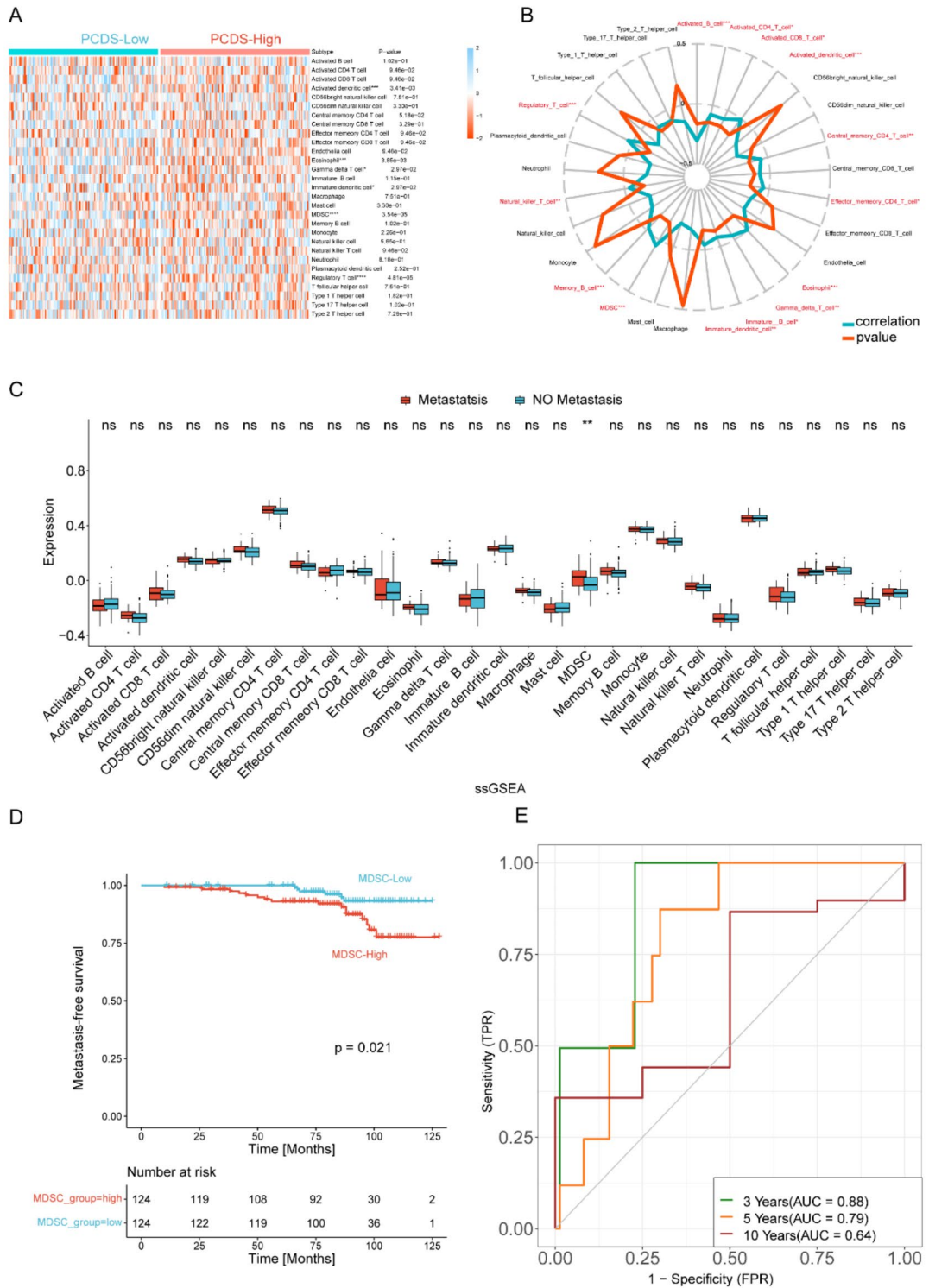


**Fig. 5.** Analysis of the tumor microenvironment. **(A)** Heatmap illustrating differences in immune cell infiltration between the high-PCDS and low-PCDS groups. **(B)** Radar plot showing the correlation between PCDS and immune cells. **(C)** Comparison of immune cell infiltration between metastasis and non-metastasis groups; **(D)** Kaplan-Meier curves were generated to show the association of MDSC with metastasis-free survival; **(E)** Time-dependent ROC curve of MDSC for metastasis. \*\*\*\* $P < 0.0001$ , \*\*\* $P < 0.001$ , \*\* $P < 0.01$ , \* $P < 0.05$ .

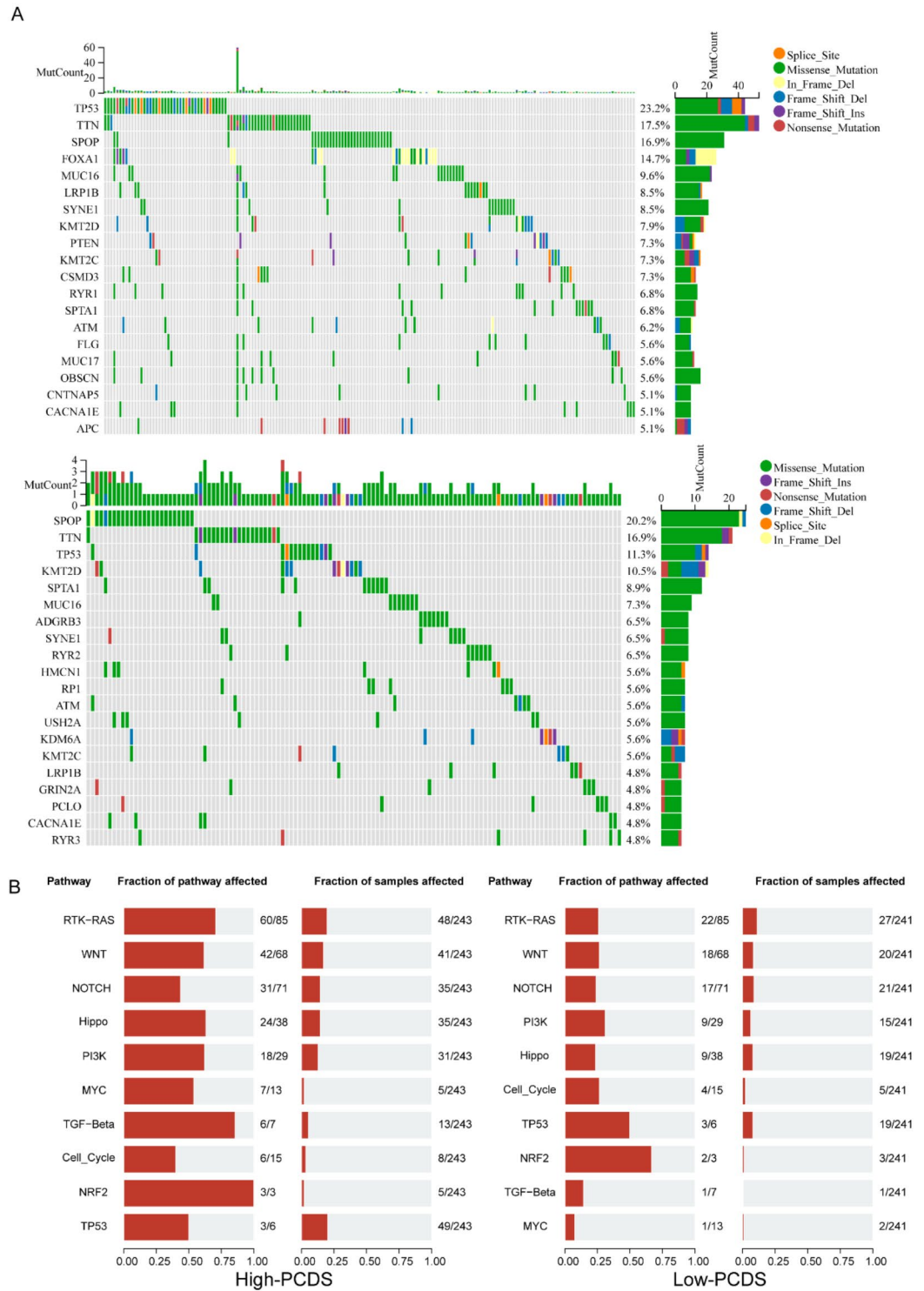


**Fig. 6.** Landscapes of somatic mutations and potential targets in the two groups. **(A)** Waterfall plot showing the mutation patterns of the top 20 most frequently mutated genes in two groups. **(B)** The fraction of pathways or samples of oncogenic signaling pathways in PCDS-high and PCDS-low groups.

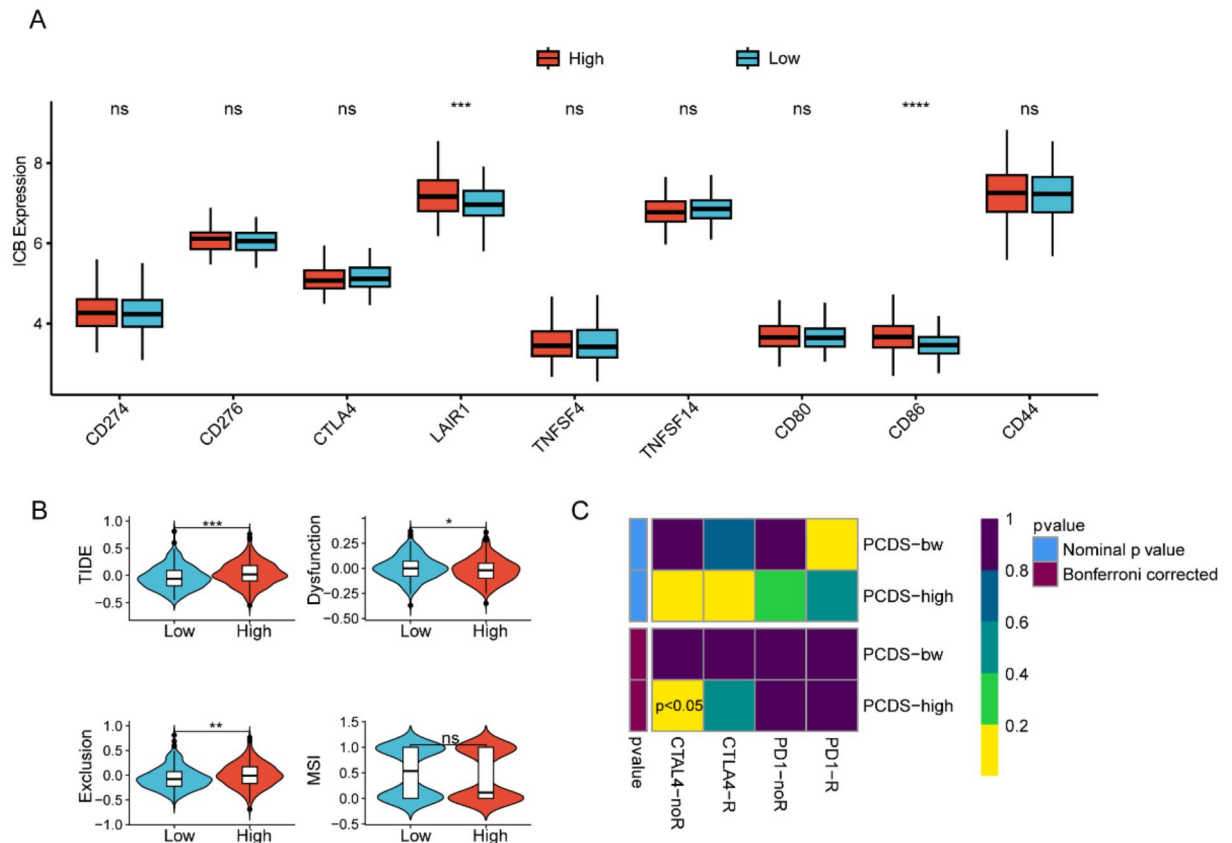


**Fig. 7.** Immunotherapy efficacy analysis. **(A)** Comparison between the PCDS-high and PCDS-low groups concerning immune checkpoint genes; **(B)** and TIDE score; **(C)** Submap analysis. \*\*\*\* $P < 0.0001$ , \*\*\* $P < 0.001$ , \*\* $P < 0.01$ , \* $P < 0.05$ , ns non-significant.

results by indicating that the likelihood of adverse medication reactions against this target and the existence of horizontal pleiotropy in PTGDS is probably low. Unfortunately, colocalization analysis suggested that PTGDS didn't share the same variant with PRAD( $PP.H4 = 0.13$ ).

### Molecular characteristics of PTGDS at single-cell sequencing level

We proceeded to investigate the PTGDS characteristics in 13 PCa samples using single-cell sequencing analysis. Through this approach, we identified a total of 8 distinct cell types: B cell, CD8Tex, endothelial, epithelial, fibroblasts, malignant, mast, and monocyte/macrophage (Fig. 10A). Remarkably, our results demonstrated a noteworthy upregulation of PTGDS expression in non-metastatic tissues, whereas metastatic tissues exhibited a comparatively lower expression of PTGDS (Fig. 10B,C). To gain further insights, we visualized the DEGs among the identified cell types, as depicted in Fig. 10D. Analysis of single-cell sequencing data using GSVA revealed that tumor cells with lower PTGDS demonstrated more pronounced malignant biological characteristics, such as angiogenesis, epithelial-to-mesenchymal transition, and Kras signaling (Fig. 10E). Additionally, we employed pseudotime trajectory analysis using monocle and observed an increase in PTGDS expression as pseudotime increased (Fig. 10F). We investigated the intercellular communication between malignant cells exhibiting high and low PTGDS expression levels. Our findings demonstrate that malignant cells with high PTGDS expression establish a greater number of interactions within the tumor microenvironment when compared to malignant cells with low PTGDS expression (Fig. 10G-H). Notably, these interactions predominantly involve immune cells and are mediated through the MK, MIF, and VISEFATIN signaling pathways (Fig. 10I-K).

### Functional analysis of PTGDS using GSEA

The biological role of PTGDS in PRAD was elucidated through GSEA. We analyzed functional HALLMARK, KEGG, and GO terms associated with PTGDS. The results revealed that the top five HALLMARK terms in the low-PTGDS group included complement, epithelial-mesenchymal transition, apoptosis, IL-6/JAK/STAT3 signaling, and KRAS signaling upregulation (Fig. 11A). In the low-PTGDS group, the top five KEGG terms were primary immunodeficiency, complement and coagulation cascades, cytokine-cytokine receptor interaction, JAK-STAT signaling pathway, and NF-kappa B signaling pathway (Fig. 11B). Additionally, the top five GO terms in the low-PTGDS group comprised epithelial cell migration, epithelial cell proliferation, immune effector process, immune receptor activity, and T cell-mediated cytotoxicity (Fig. 11C). Enrichment analyses across three

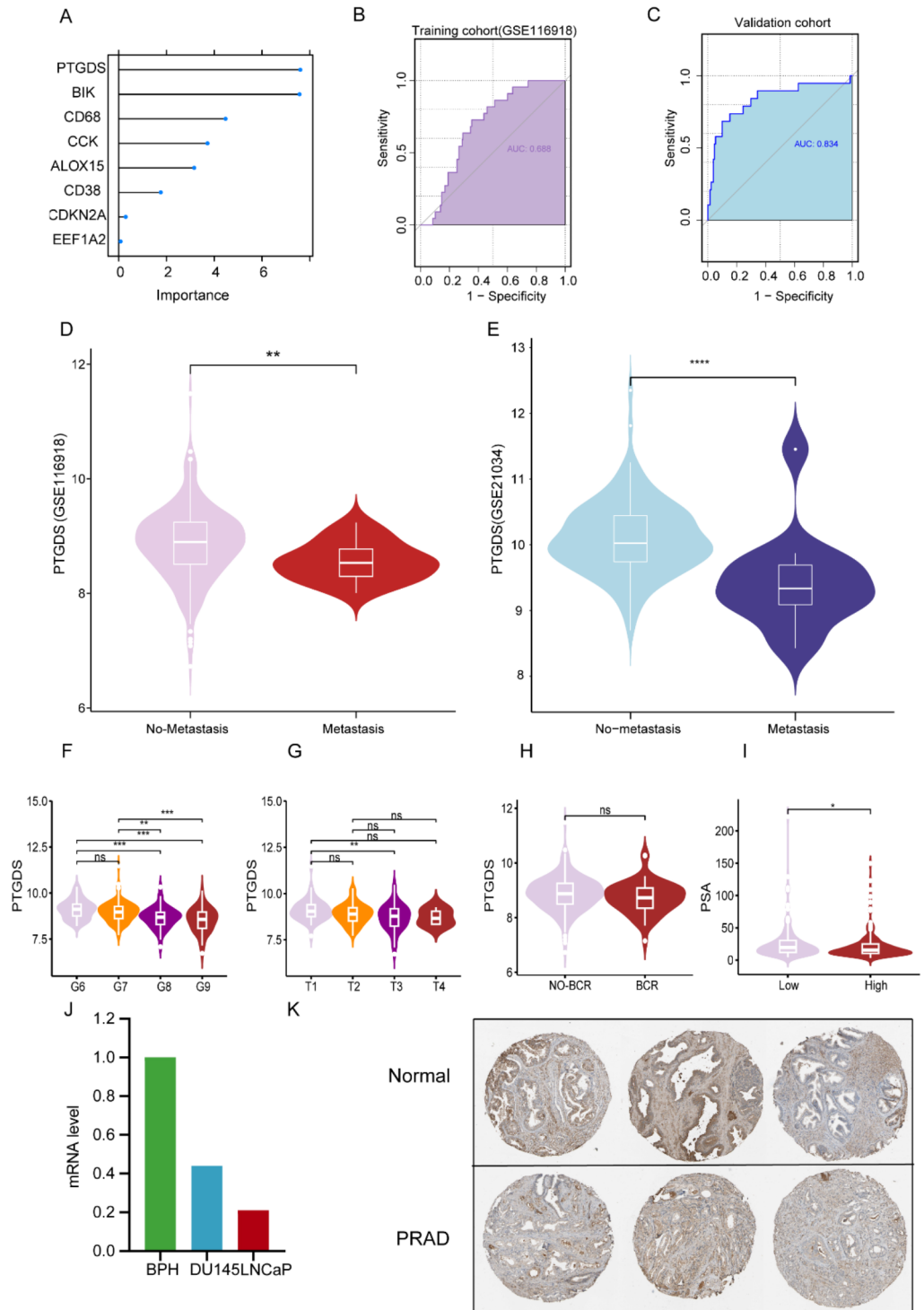


**Fig. 8.** The central role of PTGDS in PRAD. (A) Random forest analysis identifying PTGDS as core gene. ROC curve of PTGDS for metastasis in GSE116918 (B) and GSE21034 (C) cohorts. Comparison of PTGDS expression between metastasis and non-metastasis groups in GSE116918 (D) and GSE21034 (E) cohorts. Comparison of PTGDS expression with Gleason score (F), T stage (G), biochemical recurrence (H), and PSA levels (I) in GSE116918 cohort. (J) Expression levels of PTGDS detected by qRT-PCR in three cell lines. (K) Protein expression of PTGDS validated by Immunohistochemistry (IHC) based on the Human Protein Atlas (HPA) database. \*\*\*\* $P < 0.0001$ , \*\*\* $P < 0.001$ , \*\* $P < 0.01$ , \* $P < 0.05$ , *ns* non-significant.

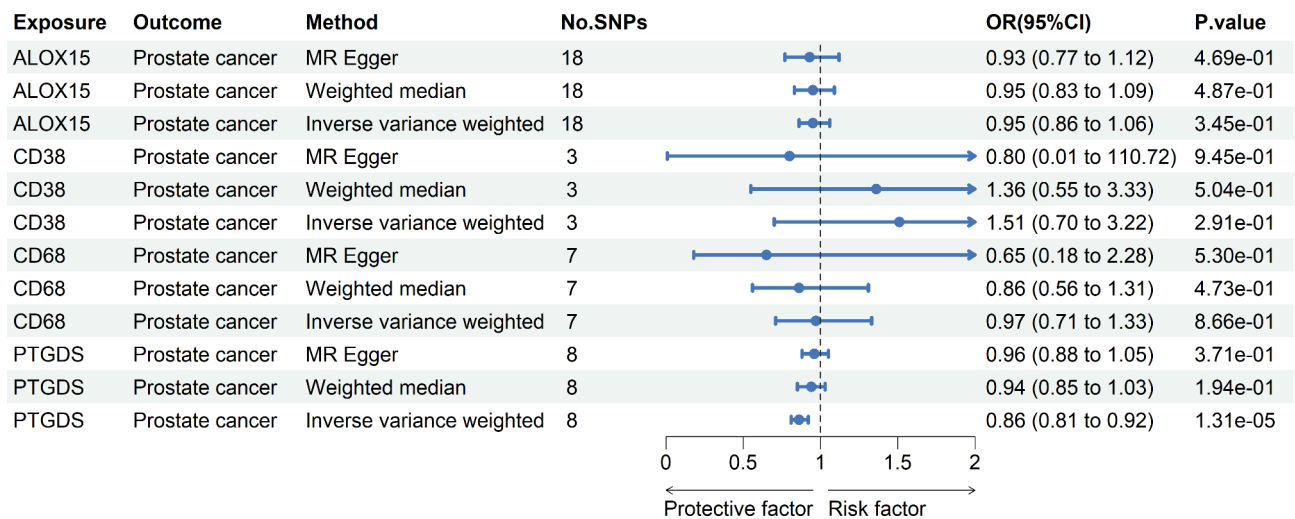


**Fig. 9.** Forest plots displaying the findings from the eQTLGen Consortium for 4 model genes.

databases consistently implicated PTGDS in EMT regulation. Validating these *in silico* predictions, correlation analysis revealed significant positive associations between PTGDS expression and epithelial markers occludin (OCLN) and E-cadherin (CDH1). Conversely, significant inverse correlations were noted with mesenchymal markers vimentin (VIM),  $\alpha$ -smooth muscle actin (ACTA2), tenascin C (TNC), and matrix metalloproteinase-2 (MMP2) (Fig. 11D).

#### PTGDS inhibited invasion, metastasis, and proliferation in PRAD

In order to get more insight into the biological function of PTGDS in PRAD cells, we increased the levels of PTGDS in DU145 and LnCaP cells, respectively (Fig. 12A, Figures S7, 8). As demonstrated by CCK-8 tests, PTGDS overexpression dramatically reduced the proliferation ability of PRAD cells (Fig. 12B). The influence of PTGDS overexpression on prostate cancer cell migration and invasiveness was appraised through wound healing and transwell assays. A substantial reduction in migratory capacity was observed in both DU145 and LnCaP cells, coupled with impaired invasion ability (Fig. 12C–H, Table S8). Collectively, these functional assays underscore the pivotal role of PTGDS as a suppressor of prostate cancer cell proliferation, invasion, and metastatic properties.

#### Discussion

PCa is generally an indolent disease with a favorable prognosis in comparison with other urological malignancies<sup>41</sup>. Nevertheless, despite surgery and radiation, around 30% of intermediate to high-risk localized and locally progressed PCa patients have recurrence or metastasis, which ultimately proves fatal<sup>3</sup>. PCD includes elaborate regulation and involves various mechanisms. Accumulating evidence indicates that PCD is integral to biological processes that have long been implicated in the proliferation and metastasis of malignant tumors<sup>19</sup>. Previous studies have utilized programmed cell death-related genes to develop prognostic models for predicting the outcomes of tumor patients or the efficacy of immunotherapy<sup>42,43</sup>. Furthermore, some studies have also developed prediction models related to prostate cancer to forecast clinical outcomes, including metastasis<sup>44</sup> and biochemical recurrence<sup>45</sup>, among prostate cancer patients. Fewer studies have, nonetheless, created a straightforward and useful genetic biomarker that uses PCD-associated markers to forecast metastases in patients receiving radical radiation treatment. This study represents the initial comprehensive analysis of thirteen distinct programmed cell death patterns in PRAD metastasis. This study represents the first comprehensive analysis of thirteen distinct PCD patterns in PRAD metastasis. In this work, we established a signature made up of eight PCD genes (ALOX15, BIK, CCK, CD38, CD68, CDKN2A, EEF1A2, and PTGDS) that exhibit strong predictive potential for both metastasis, as well as for BCR and CTRP in patients diagnosed with PRAD. Moreover, PCDS is an independent risk factor for metastasis in prostate cancer, and they demonstrate notably higher diagnostic accuracy in contrast to clinical variables like age and PSA.

Enrichment analysis indicated that pathways associated with immunity, tumors, and EMT may potentially participate in the metastasis of PCa. Over the past two decades, one of the intriguing discoveries in cancer research has been the intricate interplay between tumors and their surrounding microenvironment, also known as the tumor immune microenvironment (TIME). The TIME encompasses a variety of elements, including adjacent blood vessels, immune cells, fibroblasts, bone marrow-derived inflammatory cells, various signaling molecules, and extracellular matrix (ECM)<sup>46</sup>. Within the context of our study, we have noted that patients with prostate cancer who were categorized under the high PCDS group and the metastasis group exhibited greater infiltration of MDSCs when compared to their respective control groups. This observation implies that MDSCs could potentially facilitate the metastasis of prostate cancer. MDSCs are a diverse subset of innate immune cells that are produced from the myeloid lineage at different developmental stages. In a healthy physiological environment, they can differentiate into granulocytes, macrophages, and dendritic cells (DCs). However, the

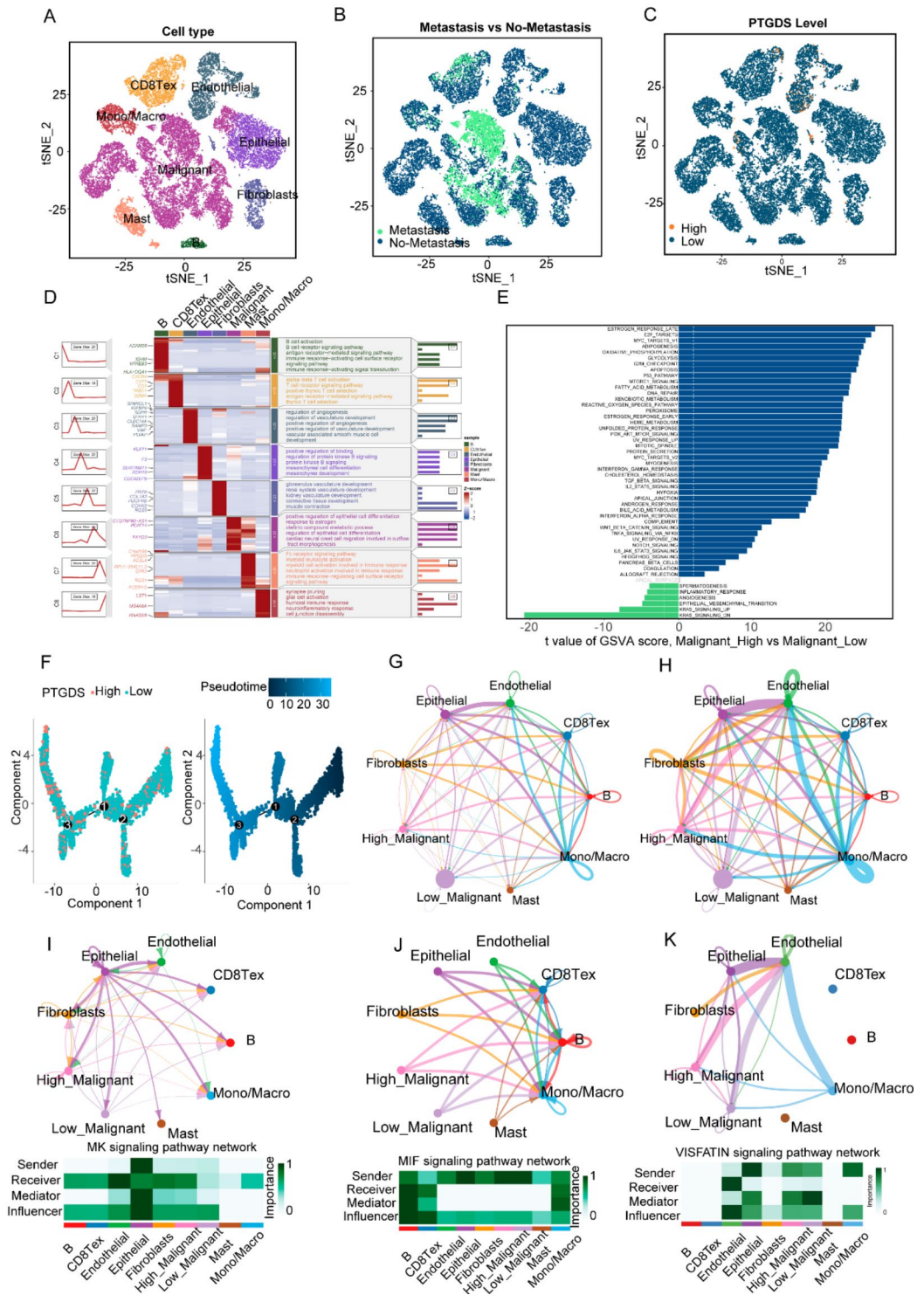


**Fig. 10.** Molecular features of PTGDS at the single-cell level. (A) t-SNE of 8 cell types; (B) t-SNE of metastasis and no-metastasis patients; (C) t-SNE of the distribution of PTGDS among different types; (D) The differentially expressed genes among the identified 8 cell types; (E) Gene set variation analysis of PRAD cells with different levels of PTGDS; (F) Pseudotime trajectory analysis based on PTGDS expression; (G) The quantity of interactions in a network of cell-cell communication; (H) The weights and strengths of the cell-to-cell communication network interactions; (I–K) Cellular interaction networks between PRAD cells with different PTGDS level and other cells in MK(I), MIF(J), and VIFATIN signaling pathway(K).

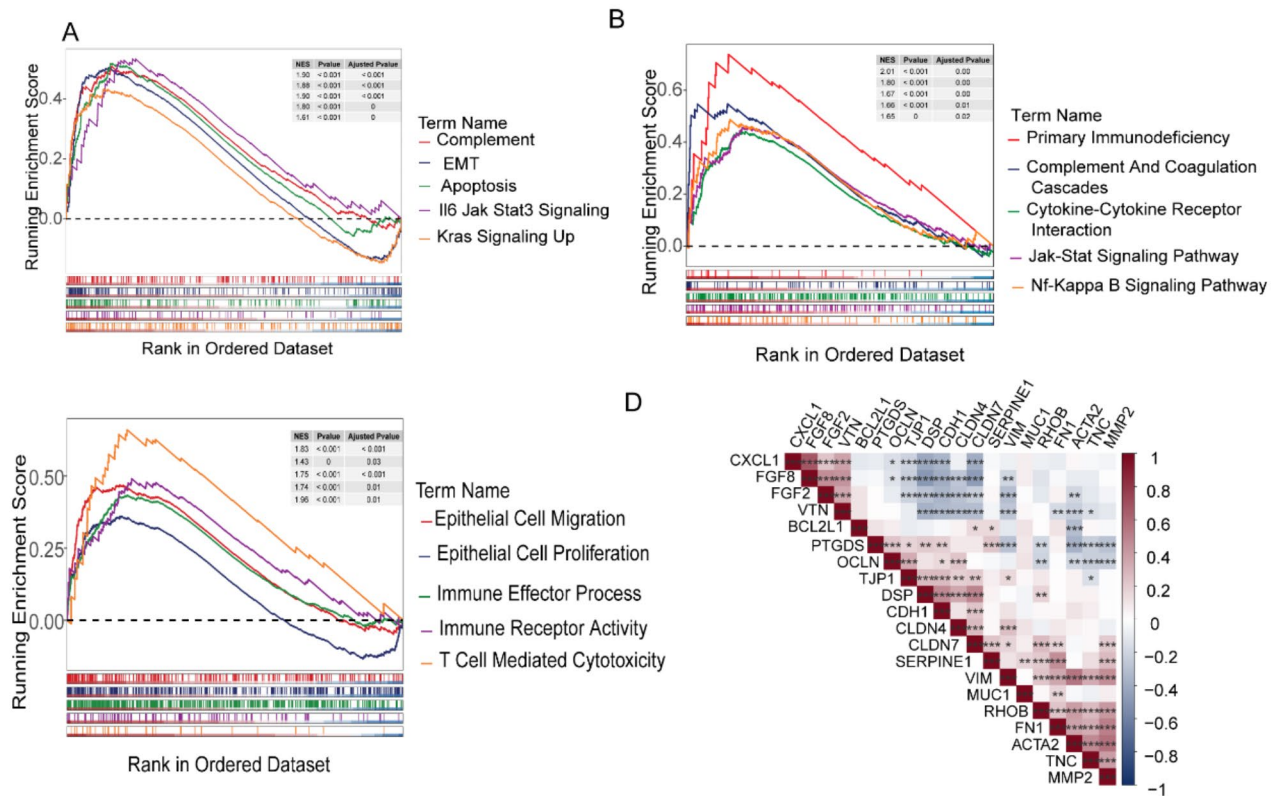


**Fig. 11.** GSEA analysis. (A) GSEA Hallmark analysis; (B) GSEA KEGG analysis; (C) GSEA GO analysis; (D) Correlation heatmap illustrating the relationship between PTGDS and EMT-related genes.

release of immunosuppressive factors impedes the differentiation of myeloid progenitors in some pathological conditions, including inflammation, trauma, tumors, and autoimmune diseases. This inhibits the immune response, which is mediated by T cells, natural killer cells, and dendritic cells; it also encourages the production of regulatory T cells and tumor-associated macrophages; it drives the immune escape; and, ultimately, it results in tumor progression and metastasis<sup>47–49</sup>. Significant variations in the mutation landscape between the high and low PCDS groups were also seen in our study, which implies that the mutation landscape may be essential to tumor metastasis.

CIT is an established and vitally significant method of cancer treatment. Numerous studies have shown that PCD is common in almost all malignancies and is closely linked to the response to CIT<sup>50–53</sup>. Considering the correlation between PCD and CIT, we utilized two datasets associated with CIT response and determined that the PCDS serves as a reliable biomarker for predicting CIT response.

Prostaglandins generated by prostate support tissues can profoundly impact cancer cell growth<sup>54</sup>. Lipocalin prostaglandin D synthetase (L-PGDS or PTGDS) resides on chromosome 9q34.2–34.3 within the lipocalin gene cluster<sup>55</sup> and possesses bifunctional enzymatic and transporter roles for PGD<sub>2</sub><sup>56</sup>. While some studies report PTGDS overexpression in melanomas, ovarian, diffuse large B-cell lymphoma, and liver tumors<sup>57–60</sup>, others find reduced PTGDS inhibits progression in lung<sup>61</sup> and gastric cancer<sup>62</sup>. However, the role of PTGDS dysregulation in prostate cancer metastasis remains undefined.

To further validate the relationship between PTGDS and prostate cancer, MR analysis of expression quantitative trait loci (eQTLs) was performed. Multiple MR methods consistently revealed significant associations between PTGDS and PCa risk, including MR-Egger, inverse variance weighted, weighted median, Cochran's Q heterogeneity test, horizontal pleiotropy assessment, bidirectional MR, Steiger filtering, colocalization analysis, and phenome-wide association study (PheWAS).

Using the random forest algorithm, we identified PTGDS as a potential core gene involved in prostate metastasis with an AUC of 0.688 in the GSE116918 cohort and 0.834 in the GSE21034 cohort. We observed a negative correlation between PTGDS expression and the presence of metastasis or BCR, as well as increasing Gleason score, T stage, and PSA levels. Transcriptomic analysis revealed significantly lower PTGDS expression in tumor tissues compared to normal tissues. This differential expression was further validated by immunohistochemistry and quantitative PCR (qPCR) analyses. Collectively, these results demonstrate an inverse relationship between PTGDS expression and tumor occurrence as well as progression.

Vanessa C. Thompson et al. highlighted the significance of the PTGDS gene in biochemical recurrence among prostate cancer patients. However, the specific molecular mechanisms underlying its impact on the prostate cancer phenotype were not elucidated, and *in vitro* experiments were not conducted<sup>45</sup>. It is widely recognized that acquiring migratory and invasive capacities represents the crucial rate-limiting initial step in



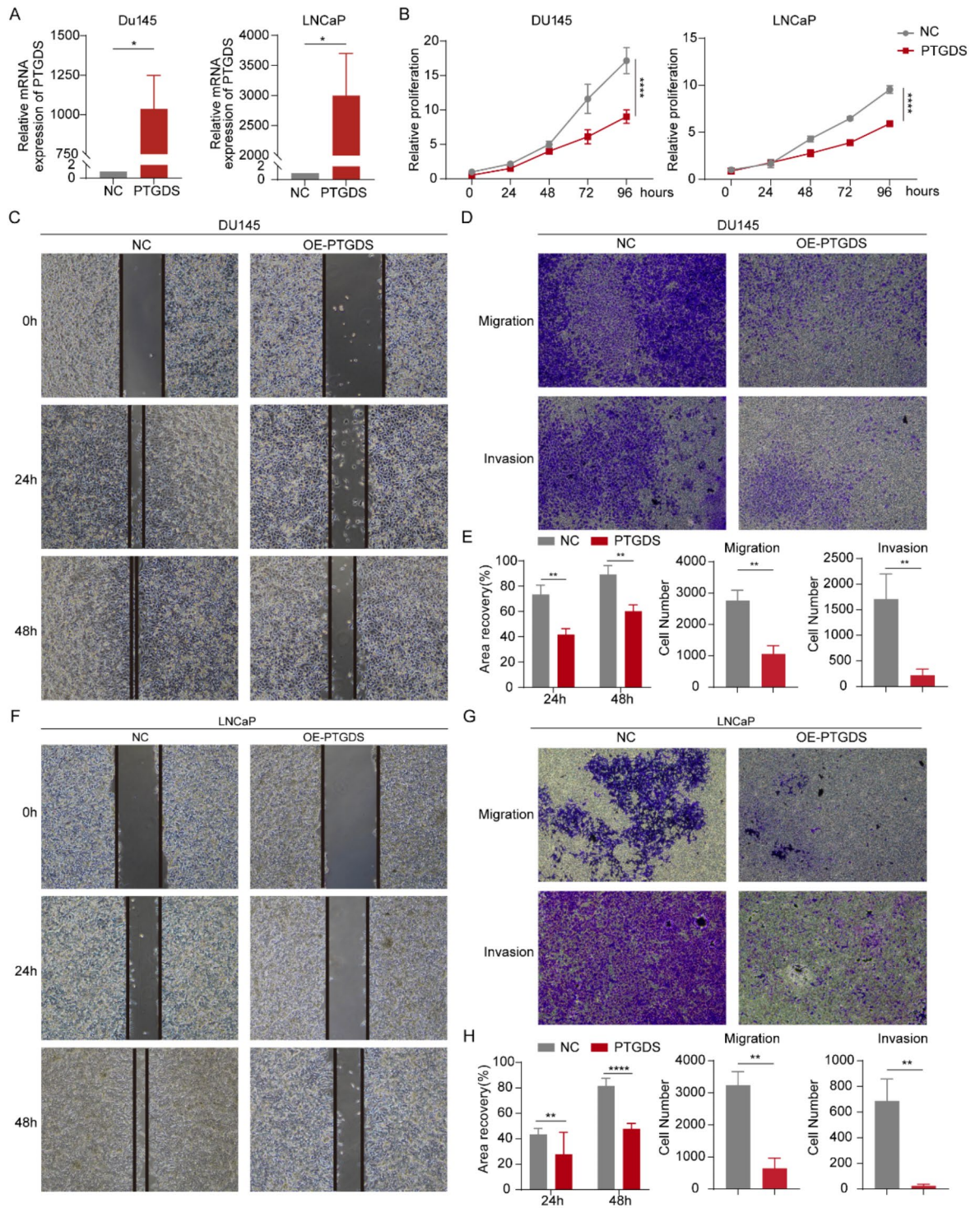


**Fig. 12.** PTGDS suppressed the proliferation, invasion, and metastasis potential of PRAD cells. (A) The effectiveness of PTGDS overexpression was verified by qRT-PCR in DU145 and LNCaP cells. (B) Cell Counting Kit-8 (CCK-8) assay to detect the proliferative capacity of PRAD cells. (C–E) Representative data from wound healing assays and transwell assays conducted with the DU145 cells. (F–H) Representative data from wound healing assays and transwell assays conducted with the LNCaP cells. \*\*\*\* $P < 0.0001$ , \*\* $P < 0.01$ , \* $P < 0.05$ , *ns* non-significant.

the metastatic cascade<sup>63</sup>. Bioinformatic analyses including GSEA, correlation, and single-cell RNA sequencing consistently linked high PTGDS expression to inhibition of EMT-related pathways. We validated these findings in vitro by developing PTGDS-overexpressing prostate cancer cell lines via plasmid transfection and verifying overexpression using RT-PCR. Strikingly, elevated PTGDS significantly suppressed cellular invasion, metastasis, and proliferation capacities. Collectively, these multi-modal results demonstrate that PTGDS acts as a protective factor in prostate cancer cells.

Despite the promising findings in this study, certain weaknesses still remain. It is widely acknowledged that gene expression signatures may be subject to sampling bias due to intratumor genetic heterogeneity. Furthermore, it is imperative that all findings in this study undergo external validation through larger sample research in order to delve deeper into the underlying mechanisms of pathogenesis. Finally, while Mendelian randomization provides insight into potential causal relationships, it assumes low-dose chronic exposure and linear dose-response links that may not fully extrapolate to real-world clinical trials that often feature short-term high-dose treatments.

## Conclusion

Our work developed a gene signature model related to PCD that can predict MFS, BCR, CTRP, and immunotherapy effectiveness in PRAD. Furthermore, we have assessed the potential predictive value of PTGDS in hindering PRAD metastasis. We believe that our findings have expanded the current knowledge on the involvement of PCD in PRAD biology and prognosis prediction and that PTGDS has the potential to serve as a novel predictive biomarker for clinical outcomes in PRAD.

## Data availability

The corresponding author can be contacted for free to receive any data or R code used in this work.

Received: 2 March 2024; Accepted: 12 September 2024

Published online: 17 September 2024

## References

- Sung, H. et al. Global Cancer statistics 2020: GLOBOCAN estimates of incidence and Mortality Worldwide for 36 cancers in 185 countries. *CA Cancer J. Clin.* **71**(3), 209–249 (2021).
- Lowenstein, L. M. et al. Active surveillance for prostate and thyroid cancers: Evolution in clinical paradigms and lessons learned. *Nat. Rev. Clin. Oncol.* **16**(3), 168–184 (2019).
- Teo, M. Y., Rathkopf, D. E. & Kantoff, P. Treatment of advanced prostate cancer. *Annu. Rev. Med.* **70**, 479–499 (2019).
- Matsumoto, K. et al. Establishment of the optimal follow-up schedule after radical prostatectomy. *Urol. Oncol.* **36**(7), 341 (2018).
- Pound, C. R. et al. Natural history of progression after PSA elevation following radical prostatectomy. *Jama* **281**(17), 1591–1597 (1999).
- Han, M., Partin, A. W., Pound, C. R., Epstein, J. I. & Walsh, P. C. Long-term biochemical disease-free and cancer-specific survival following anatomic radical retropubic prostatectomy. The 15-year Johns Hopkins experience. *Urol. Clin. North. Am.* **28**(3), 555–565 (2001).
- Ward, J. F., Blute, M. L., Slezak, J., Bergstralh, E. J. & Zincke, H. The long-term clinical impact of biochemical recurrence of prostate cancer 5 or more years after radical prostatectomy. *J. Urol.* **170**(5), 1872–1876 (2003).
- Roehl, K. A., Han, M., Ramos, C. G., Antenor, J. A. & Catalona, W. J. Cancer progression and survival rates following anatomical radical retropubic prostatectomy in 3,478 consecutive patients: Long-term results. *J. Urol.* **172**(3), 910–914 (2004).
- Bubendorf, L. et al. Metastatic patterns of prostate cancer: an autopsy study of 1,589 patients. *Hum. Pathol.* **31**(5), 578–583 (2000).
- Rycaj, K., Li, H., Zhou, J., Chen, X. & Tang, D. G. Cellular determinants and microenvironmental regulation of prostate cancer metastasis. *Semin Cancer Biol.* **44**, 83–97 (2017).
- Beer, T. M. et al. Enzalutamide in metastatic prostate cancer before chemotherapy. *N. Engl. J. Med.* **371**(5), 424–433 (2014).
- de Bono, J., Kang, J. & Hussain, M. Olaparib for metastatic castration-resistant prostate Cancer. Reply. *N Engl. J. Med.* **383**(9), 891 (2020).
- Hussain, M. et al. Survival with Olaparib in Metastatic Castration-resistant prostate Cancer. *N Engl. J. Med.* **383**(24), 2345–2357 (2020).
- Wurz, G. T., Kao, C. J. & DeGregorio, M. W. Novel cancer antigens for personalized immunotherapies: Latest evidence and clinical potential. *Ther. Adv. Med. Oncol.* **8**(1), 4–31 (2016).
- Fong, L. et al. Activated lymphocyte recruitment into the tumor microenvironment following preoperative sipuleucel-T for localized prostate cancer. *J. Natl. Cancer Inst.* **106**(11), (2014).
- Beer, T. M. et al. Randomized, Double-Blind, phase III trial of Ipilimumab Versus Placebo in Asymptomatic or minimally symptomatic patients with metastatic chemotherapy-naïve castration-resistant prostate Cancer. *J. Clin. Oncol.* **35**(1), 40–47 (2017).
- Hegde, P. S. & Chen, D. S. Top 10 challenges in Cancer Immunotherapy. *Immunity* **52**(1), 17–35 (2020).
- Tang, D., Kang, R., Berghe, T. V., Vandenabeele, P. & Kroemer, G. The molecular machinery of regulated cell death. *Cell. Res.* **29**(5), 347–364 (2019).
- Su, Z., Yang, Z., Xu, Y., Chen, Y. & Yu, Q. Apoptosis, autophagy, necroptosis, and cancer metastasis. *Mol. Cancer* **14**, 48 (2015).
- Liang, J. L. et al. Specific activation of cGAS-STING pathway by nanotherapeutics-mediated ferroptosis evoked endogenous signaling for boosting systemic tumor immunotherapy. *Sci. Bull. (Beijing)* (2023).
- Jain, S. et al. Validation of a metastatic assay using biopsies to improve risk stratification in patients with prostate cancer treated with radical radiation therapy. *Ann. Oncol.* **29**(1), 215–222 (2018).
- Taylor, B. S. et al. Integrative genomic profiling of human prostate cancer. *Cancer Cell* **18**(1), 11–22 (2010).
- Friedrich, M. et al. The role of lncRNAs TAPIR-1 and -2 as diagnostic markers and potential therapeutic targets in prostate Cancer. *Cancers (Basel)* **12**(5), (2020).
- Grasso, C. S. et al. The mutational landscape of lethal castration-resistant prostate cancer. *Nature* **487**(7406), 239–243 (2012).
- Sharma, N. L. et al. The androgen receptor induces a distinct transcriptional program in castration-resistant prostate cancer in man. *Cancer Cell* **23**(1), 35–47 (2013).
- Kanehisa, M., Furumichi, M., Sato, Y., Kawashima, M. & Ishiguro-Watanabe, M. KEGG for taxonomy-based analysis of pathways and genomes. *Nucleic Acids Res.* **51**(D1), D587–D92 (2022).
- Kanehisa, M. Toward understanding the origin and evolution of cellular organisms. *Protein Sci.* **28**(11), 1947–1951 (2019).
- Kanehisa, M. & Goto, S. KEGG: Kyoto Encyclopedia of genes and genomes. *Nucleic Acids Res.* **28**(1), 27–30 (2000).

29. Yu, G., Wang, L. G., Han, Y. & He, Q. Y. clusterProfiler: An R package for comparing biological themes among gene clusters. *Omics* **16**(5), 284–287 (2012).
30. Jia, Q. et al. Local mutational diversity drives intratumoral immune heterogeneity in non-small cell lung cancer. *Nat. Commun.* **9**(1), 5361 (2018).
31. Mayakonda, A., Lin, D. C., Assenov, Y., Plass, C. & Koeffler, H. P. Maftools: Efficient and comprehensive analysis of somatic variants in cancer. *Genome Res.* **28**(11), 1747–1756 (2018).
32. Jin, S. et al. Inference and analysis of cell-cell communication using CellChat. *Nat. Commun.* **12**(1), 1088 (2021).
33. Kurki, M. I. et al. FinnGen provides genetic insights from a well-phenotyped isolated population. *Nature* **613**(7944), 508–518 (2023).
34. Hemani, G. et al. The MR-Base platform supports systematic causal inference across the human phenome. *Elife* **7** (2018).
35. Hemani, G., Tilling, K. & Davey Smith, G. Orienting the causal relationship between imprecisely measured traits using GWAS summary data. *PLoS Genet.* **13**(11), e1007081 (2017).
36. Giambartolomei, C. et al. Bayesian test for colocalisation between pairs of genetic association studies using summary statistics. *PLoS Genet.* **10**(5), e1004383 (2014).
37. Foley, C. N. et al. A fast and efficient colocalization algorithm for identifying shared genetic risk factors across multiple traits. *Nat. Commun.* **12**(1), 764 (2021).
38. Wang, Q. et al. Rare variant contribution to human disease in 281,104 UK Biobank exomes. *Nature* **597**(7877), 527–532 (2021).
39. Bruni, D., Angell, H. K. & Galon, J. The immune contexture and immunoscore in cancer prognosis and therapeutic efficacy. *Nat. Rev. Cancer* **20**(11), 662–680 (2020).
40. Gerstberger, S., Jiang, Q. & Ganesh, K. Metastasis. *Cell* **186**(8):1564–1579. (2023).
41. Feng, D. et al. Developing an immune-related gene prognostic index associated with progression and providing new insights into the tumor immune microenvironment of prostate cancer. *Immunology* **166**(2), 197–209 (2022).
42. Huang, Y. et al. A comprehensive analysis of programmed cell death-Associated genes for Tumor Microenvironment evaluation promotes precise immunotherapy in patients with Lung Adenocarcinoma. *J. Pers. Med.* **13**(3). (2023).
43. Chen, B. et al. An integrated machine learning framework identifies prognostic gene pair biomarkers associated with programmed cell death modalities in clear cell renal cell carcinoma. *Front. Biosci. (Landmark Ed)* **29**(3), 121 (2024).
44. Feng, D. et al. Immune-related gene index predicts metastasis for prostate cancer patients undergoing radical radiotherapy. *Exp. Hematol. Oncol.* **12**(1), 8 (2023).
45. Thompson, V. C. et al. A gene signature identified using a mouse model of androgen receptor-dependent prostate cancer predicts biochemical relapse in human disease. *Int. J. Cancer* **131**(3), 662–672 (2012).
46. Hanahan, D. & Weinberg, R. A. Hallmarks of cancer: The next generation. *Cell* **144**(5), 646–674 (2011).
47. Krystal, G. et al. Re: The terminology issue for myeloid-derived suppressor cells. *Cancer Res.* **67**(8), 3986 (2007).
48. Rodrigues, J. C. et al. Normal human monocytes exposed to glioma cells acquire myeloid-derived suppressor cell-like properties. *Neuro Oncol.* **12**(4), 351–365 (2010).
49. Movahedi, K. et al. Identification of discrete tumor-induced myeloid-derived suppressor cell subpopulations with distinct T cell-suppressive activity. *Blood* **111**(8), 4233–4244 (2008).
50. Gu, X., Liu, Y., Dai, X., Yang, Y. G. & Zhang, X. Deciphering the potential roles of ferroptosis in regulating tumor immunity and tumor immunotherapy. *Front. Immunol.* **14**, 1137107 (2023).
51. Jiang, A. et al. A new thinking: Deciphering the aberrance and clinical implication of copper-death signatures in clear cell renal cell carcinoma. *Cell. Biosci.* **12**(1), 209 (2022).
52. Nan, Z. et al. Identification and validation of a prognostic signature of autophagy, apoptosis and pyroptosis-related genes for head and neck squamous cell carcinoma: to imply therapeutic choices of HPV negative patients. *Front. Immunol.* **13**, 1100417 (2022).
53. Su, W., Hong, T., Feng, B., Yang, Z. & Lei, G. A unique regulated cell death-related classification regarding prognosis and immune landscapes in non-small cell lung cancer. *Front. Immunol.* **14**, 1075848 (2023).
54. Kim, J. et al. Suppression of prostate tumor cell growth by stromal cell prostaglandin D synthase-derived products. *Cancer Res.* **65**(14), 6189–6198 (2005).
55. Irikura, D. et al. Biochemical, functional, and pharmacological characterization of AT-56, an orally active and selective inhibitor of lipocalin-type prostaglandin D synthase. *J. Biol. Chem.* **284**(12), 7623–7630 (2009).
56. Urade, Y. & Hayaishi, O. Biochemical, structural, genetic, physiological, and pathophysiological features of lipocalin-type prostaglandin D synthase. *Biochim. Biophys. Acta* **1482**(1–2), 259–271 (2000).
57. Shimanuki, M., Takeda, K., Kawaguchi, M., Suzuki, T. & Shibahara, S. Lipocalin-type prostaglandin D synthase as a marker for the proliferative potential of melanocyte-lineage cells in the human skin. *J. Dermatol.* **39**(8), 699–704 (2012).
58. Lim, W. et al. Prostaglandin D<sub>2</sub> synthase related to estrogen in the female reproductive tract. *Biochem. Biophys. Res. Commun.* **456**(1), 355–360 (2015).
59. Hu, S. et al. Glycoprotein PTGDS promotes tumorigenesis of diffuse large B-cell lymphoma by MYH9-mediated regulation of Wnt-β-catenin-STAT3 signaling. *Cell. Death Differ.* **29**(3), 642–656 (2022).
60. Nault, J. C. et al. Argininosuccinate synthase 1 and periportal gene expression in sonic hedgehog hepatocellular adenomas. *Hepatology* **68**(3), 964–976 (2018).
61. Ragolia, L., Palaia, T., Hall, C. E., Klein, J. & Büyük, A. Diminished lipocalin-type prostaglandin D(2) synthase expression in human lung tumors. *Lung Cancer* **70**(1), 103–109 (2010).
62. Zhang, B. et al. PGD2/PTGDR2 signaling restricts the Self-Renewal and Tumorigenesis of Gastric Cancer. *Stem Cells* **36**(7), 990–1003 (2018).
63. De Craene, B. & Berx, G. Regulatory networks defining EMT during cancer initiation and progression. *Nat. Rev. Cancer* **13**(2), 97–110 (2013).

## Author contributions

DPW, NH and YFD contributed to the conception of the study. BHC designed the study and wrote the manuscript. Visualization and experiments in vitro were performed by BHC, LG, LHW, XYS, PQW, XYZ, CZT and MGZ. MGZ, HXH, YYL, NX and BHC collected the data in the study and take responsibility for the integrity of the data. BHC and KY performed the statistical analyses. All authors contributed to the article and approved the submitted version. All authors read and approved the final manuscript.

## Funding

This study was funded by the Beijing Bethune Charitable Foundation (Special research fund for urinary tumors NO.HX202184) and Funding Program No. XJTU1AF-CRF-2020-018.

## Declarations

### Competing interests

The authors declare no competing interests.

### Additional information

**Supplementary Information** The online version contains supplementary material available at <https://doi.org/10.1038/s41598-024-72985-w>.

**Correspondence** and requests for materials should be addressed to D.W. or Y.D.

**Reprints and permissions information** is available at [www.nature.com/reprints](http://www.nature.com/reprints).

**Publisher's note** Springer Nature remains neutral with regard to jurisdictional claims in published maps and institutional affiliations.

**Open Access** This article is licensed under a Creative Commons Attribution-NonCommercial-NoDerivatives 4.0 International License, which permits any non-commercial use, sharing, distribution and reproduction in any medium or format, as long as you give appropriate credit to the original author(s) and the source, provide a link to the Creative Commons licence, and indicate if you modified the licensed material. You do not have permission under this licence to share adapted material derived from this article or parts of it. The images or other third party material in this article are included in the article's Creative Commons licence, unless indicated otherwise in a credit line to the material. If material is not included in the article's Creative Commons licence and your intended use is not permitted by statutory regulation or exceeds the permitted use, you will need to obtain permission directly from the copyright holder. To view a copy of this licence, visit <http://creativecommons.org/licenses/by-nc-nd/4.0/>.

© The Author(s) 2024, corrected publication 2024